optica

Surface-enhanced gallium arsenide photonic resonator with a quality factor of 6 × 10^6: supplementary material

BISWARUP GUHA,[1] FELIX MARSAULT,[2] FABIAN CADIZ,[3] LAURENCE MORGENROTH,[4] VLADIMIR ULIN,[5] VLADIMIR BERKOVITZ,[5] ARISTIDE LEMAÎTRE,[2] CARMEN GOMEZ,[2] ALBERTO AMO,[2] SYLVAIN COMBRIÉ,[6] BRUNO GÉRARD,[7] GIUSEPPE LEO,[1] AND IVAN FAVERO[1,*]

[1]*Matériaux et Phénomènes Quantiques, Université Paris Diderot, CNRS UMR 7162, Sorbonne Paris-Cité, 10 rue Alice Domon et Léonie Duquet, 75013 Paris, France*

[2]*Laboratoire de Photonique et de Nanostructures, CNRS UPR 20, Route de Nozay, 91460 Marcoussis, France*

[3]*Laboratoire de Physique de la Matière Condensée, Ecole Polytechnique, CNRS UMR 7643, Route de Saclay, 91128 Palaiseau, France*

[4]*Institut d'Electronique, de Microélectronique et de Nanotechnologie, UMR CNRS 8520, Avenue Poincaré, 59652 Villeneuve d'Ascq*

[5]*A. F. Ioffe Physico-Technical Institute, 194021 Saint Petersburg, Russia*

[6]*Thales Research and Technology, Route Départementale 128, 91767 Palaiseau, France*

[7]*III-V Lab, 1 Avenue Augustin Fresnel, 91767 Palaiseau, France*

**Corresponding author: ivan.favero@univ-paris-diderot.fr*

Published 9 February 2017

This document provides supplementary information to the article "Surface-enhanced gallium arsenide photonic resonator with a quality factor of 6 × 10^6," https://doi.org/10.1364/optica.4.000218.

https://doi.org/10.1364/optica.4.000218.s001

Wet nitridation of GaAs disk optical resonators. Thin layers of GaN are interesting candidates for GaAs surface passivation thanks to the high stability of GaN bonds. In addition, because of their high electronegativity, nitrogen atoms bonded onto surface gallium atoms should not lead to electronic states within the gap of GaAs. To form a thin nitride film, a wet chemical nitridation procedure has been developed [1,2]. It consists in treating the GaAs crystal in a highly alkaline (pH=12) hydrazine (N_2H_4) solution with a small amount (0.01M) of sodium sulfide (Na_2S) added. The latter removes surface arsenic atoms under the form of soluble thioarsenic acid H_3AsS_3. The surface nitridation proceeds through dissociative adsorption of hydrazine molecules on the opened gallium atoms. The process stops after the formation of a continuous monolayer of GaN [2]. The formed nitride monolayer protects the crystal surface against oxidation. Unfortunately, the process also comes with surface microetching, which can affect the morphology of miniature structures [2,3]. This parasitic etching originates from the interaction of hydroxyl anions OH^- with surface gallium atoms. To circumvent this problem, here we intentionally decreased the pH of the hydrazine–sulfide solution down to a value of 8.5. The preparation of the solution consists in two steps: firstly, we obtain a hydrazine buffer solution by adding anhydrous hydrazine-dihydrochloride (N_2H_4×2HCl) to hydrazine-hydrate, until reaching a target pH value. Secondly, Na_2S is introduced into the solution up to a concentration of 0.01 M, leading to a concentration of OH^- anions lowered by 4 orders of magnitude and a negligible parasitic etching [4]. The finally obtained parasitic etching amounts to few nanometers to few tens of nanometers at the surface of our resonators, and can be quantified by measuring the shifts of WGMs resonances after treatment.

Before nitridation, the samples supporting GaAs disk resonators were rinsed in methylene chloride (CH_2Cl_2) and acetone, and immersed in concentrated NH_4OH solution (35%) for a few minutes before rinsing with water. After drying they were immersed in the low alkaline hydrazine-sulfide solution for 10 minutes at 80°C. The samples were subsequently rinsed in deionized water.

Time-resolved photoluminescence of GaAs disks. Room-temperature photoluminescence experiments are performed using a pulsed Ti:sapphire laser delivering 3 ps pulses at a repetition rate of 82MHz. A microscope objective 50x (NA=0.65) is used both to focus the laser on a 2 µm spot and to collect the emission, which is focused on a monochromator slit with a lens of 300 mm focal length. The emitted signal is dispersed in the monochromator and time resolved using a streak camera. A broadband long-pass filter with a cutoff wavelength of 780 nm prevents the excitation laser at 775 nm from reaching the detector. The collected room-temperature luminescence is centered at 870 nm and extends over 40 nm of wavelength span. The time-trace shown in Fig 1d of the main text is obtained by spectrally integrating the signal over this window. A schematics of the experiment is provided below.

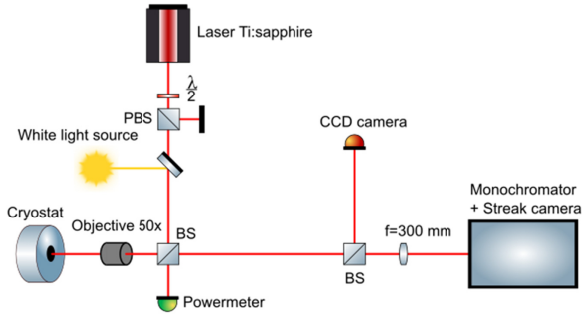

Fig. S1. Time-resolved photoluminescence experiments. PBS: Polarization Beam-Splitter. BS: Beam-splitter. The cryostat temperature is kept at room temperature in this work.

As written in the text, the decay of luminescence if fitted by a sum of three exponential functions, with respective decay times τ_1, τ_2 and τ_3. In the main text, we highlight the intermediate time (τ_2) because it corresponds to the decay of the quasi-equilibrium population of "luminescent" carriers (those close enough to k=0 in the band structure to give rise to luminescence). The two other times (short (τ_1) and long (τ_3)) are more involved to discuss but advanced interpretation has been developed in prior works [5,6]. The rapid decay (τ_1) is associated to a thermalization of optically generated carriers, with the following picture. Firstly, optical phonons allow quasi-instantaneous relaxation of generated carriers down in the bands close to k=0 in the Brillouin zone. Secondly, these carriers thermalize and hence distribute over larger-k states, reducing the occupation of states close to k=0 that are responsible of luminescence at the band-edge energy. The consequence is a first decay of the luminescence. In our experiments, this first rapid decay τ_1 is barely modified by the nitridation treatment (see table S1 below), which is consistent with the idea that this thermalization process is a bulk property, and not associated to resonator surfaces. The long time (τ_3) is typically present in the luminescence dynamics of high-quality samples, where carriers can distribute over a large span of k-numbers, even out of the light emission cone, which can increase their lifetime. Because the luminescence signal is acquired over 170 ps in our study, we lack information to precisely estimate τ_3, which generally dwells in the several hundreds of ps. For this reason, it is difficult to precisely assess the effect of nitridation on τ_3 (see table S1).

With our limited precision, we cannot conclude if the nitridation modifies τ_3 or not. Of interest if finally the rise time of the luminescence, which was unambiguously attributed to the recombination of unbound electron-hole pairs in [5]. The rise time was evaluated by fitting the rising part of the luminescence with a single growing exponential, and is also reported in table S1. It barely varies, irrespective of the excitation power (60 or 100 µW), of the fact that we collect the luminescence on a disk or on the substrate, or of the fact that the sample has been nitridated or not. Again, these observations are consistent with the idea that the rise time is a bulk property. Finally the intermediate decay time τ_2 is the only alone to clearly vary with nitridation, on average increasing from 7.7 to 18 ps on investigated disks, and from 13.8 to 17 ps on the GaAs substrate.

Mean	Before nitridation			After nitridation		
	Power (µW)	Disk	Substrate	Power (µW)	Disk	Substrate
Rise time (ps)	60	4.8±0.1		60	4.2±0.2	
	100	4.1±0.7	4.2±0.1	100	5±0.8	4±1
1st decay τ_1 (ps)	60			60	2.5±0.5	
	100	3.45±1.1	2.8±0.8	100	3±1	
2nd decay τ_2 (ps)	60			60	17.5±4.5	
	100	7.7±1	13.8±0.1	100	18±3	17±3
3rd decay τ_3 (ps)	60			60	466±248	
	100	472±394	580±30	100	163±80	390±340

Table S1. Mean values of the four times evaluated from the luminescence dynamics at room temperature, obtained by averaging over our complete data set. The data are sorted by excitation power (60 or 100 µW), by item (disk or substrate) and by surface state (before or after nitridation).

Atomic Layer Deposition on GaAs disk resonators. In this work, the ALD coating was deposited using a TFS 200 reactor (Beneq Oy). Before transferring the samples into the ALD reactor chamber, their surface was prepared under nitrogen atmosphere. The samples were first rinsed with acetone and with isopropanol. They were sometimes immersed in a NH4OH solution (6%, 20 to 30 seconds typically), before rinsing in deionized water. We noted that this ammonia pre-treatment had little impact of the final optical performance, hence part of our GaAs disks did not go through this treatment (Fig. 3 (a) and (b) of main text for example). After drying, the samples received hydrogen plasma pre-treatment in order to improve the interfacial quality, before using a plasma-enhanced atomic layer deposition (PE-ALD), in order to deposit a layer of alumina. ALD itself consists in a series of ALD cycles, which are made up of a sequence of four pulses in rapid succession: alternating pulses of precursor, here trimethyl-aluminium $Al(CH_3)_3$, and reactant, here O_2 plasma. Between precursor and reactant pulses the chamber is purged by a 300sccm flow of argon gas. Depositions were performed at a temperature of 300 °C. The number of precursor cycles for each deposition was calculated using a growth rate per cycle of ~ 0.1 nm/cycle for alumina.

Identification of whispering gallery modes. In Fig. 2 of main text, all observed WGMs are TE polarized. Their identification is reported in Fig. S2, where their radial p number goes from 1 to 6. The spectrum has been acquired at larger optical power compared to Fig. 2 of main text, in order to improve the signal to noise ratio and make the modes p=1 and 2 more clearly visible, while they are close to the noise floor at the low power required for the resonances to remain lorentzian (in the experimental conditions of Fig. 2). In the apparent resonances, and for the dimensions of the considered disks, only the p=6 modes have their Q factor bound by bending losses to a value of about a million, while the effect of bending losses on modes p=1 to 5 is basically negligible in the present work [7].

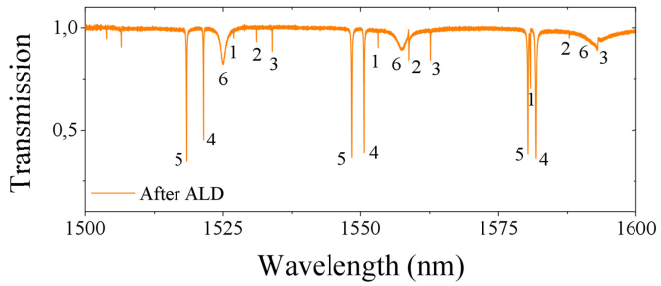

Fig. S2. Identification of the radial number p of the WGMs shown in Fig. 2 of the main text.

p	Modal confinement factor	Q_l^{before}	Q_l^{after}	Mode profile
1	0.085	Not measurable	5.2×10^5 *resolution limited	
2	0.083	70493	1.7×10^5	
3	0.081	31205	67,940	
4	0.079	15180	15,663	
5	0.076	6700	12,700	
6	0.068	1401	1462	

Table S2. Effect of ALD on the Q of modes shown in Fig. 2 of main text, function of the radial p number of the mode. A modal confinement factor is shown, which is the ratio between the electromagnetic energy confined at the surface (within a thickness of +-10 nm) and the energy confined in the whole mode. The larger the confinement factor, the more surface absorption can be anticipated.

Impact of ALD on absorption and scattering losses. On the first WGM of Fig. 3 (a) and (b), we observe an ALD-induced Q improvement of 2.33, for a "moderate" loaded Q that starts at 18 000 and rises up to 42500 after ALD. The loaded Qs being compared at equal contrast of the resonance, this improvement factor also holds for the intrinsic Q factors Q_{in}. For this "moderate Q" mode, optical dissipation prior to ALD may not be solely governed by absorption, and scattering losses may also matter, such that we can write the intrinsic Q as $Q_{in}^{-1}= Q_{abs}^{-1} +Q_{scatt}^{-1}=\alpha Q_{in}^{-1} +(1-\alpha)\ Q_{in}^{-1}$ with α an unknown parameter (with $0<\alpha<1$). After ALD, the absorption rate is multiplied by a (with $0<a<1$) and the scattering loss rate by s ($0<s<1$). In consequence, after ALD the Q becomes $(Q_{in}^{-1})^{ALD}= a.Q_{abs}^{-1} +s.Q_{scatt}^{-1}=[a\alpha+s(1-\alpha)]\ Q_{in}^{-1}$. Hence a first relation obtained from our measurements of Qs before and after ALD is that $[a\alpha+s(1-\alpha)]=(1/2.33)$. A second relation is obtained from the change in the thermo-optic shift for that WGM, which was measured at higher power to be of 47 to 54 pm. The shift being linearly proportional to the temperature increase within the disk, this change implies a change by the same amount of P_{abs}, the optical power absorbed within the disk. P_{abs} is the product of the absorption by the circulating power inside the disk, such that for a given contrast of the optical resonance the scaling is $P_{abs} \sim Q_{abs}^{-1} Q_{in}$. After ALD, we hence modify the absorbed power in the following way $(P_{abs})^{ALD} \propto (a/[a\alpha+s(1-\alpha)])\ P_{abs}$, which leads to a second relation $a/[a\alpha+s(1-\alpha)]=(54/47)$. Out of the two relations, we directly obtain $a=54/(2.33\times47)=0.49$, which means that ALD reduces absorption by a factor 2. We also obtain a complementary relation linking α and s: $\alpha=[(1/2.33)-s]/[0.49-s]$. For α and s between 0 and 1, this relation enforces $0<s<0.43$ and $0<\alpha<0.88$, which correspond to two limit cases. The first limit case (s=0 and $\alpha=0.88$) means that most of the dissipation before ALD is due to absorption: in this case, after ALD, scattering losses may be reduced (s coming close to 0) but this reduction has little impact on Q and it is mainly the reduction of absorption by a factor 2 that leads to the Q improvement of 2.33. The second limit case (s=0.43 and α close to zero) means most of the dissipation before ALD is due to scattering losses. After ALD, a reduction of scattering losses by a factor 2.33 (s=0.43) can explain the Q improvement, while the absorption is also reduced by a factor 2 and explains the new thermo-optic shift. Our measurements cannot distinguish between these two limit cases. For the second WGM of Fig. 3 (c) and (d), the same reasoning as above applies equally and leads to a=0.13, $0.86<s<1$ and $0<\alpha<0.16$, for a very modest measured Q improvement of 16 %. This means that ALD strongly reduces absorption, by a factor 7.7 (=1/0.13), but barely changes scattering losses ($0.86<s<1$). Because the Q was set by scattering losses prior to ALD ($0<\alpha<0.16$), it is little affected by the surface treatment.

From these examples we see that there are different scenarios for WGMs of "moderate Q". In first cases, absorption dominates the optical dissipation and rules the Q improvement; the impact of ALD on scattering losses, whatever it is, turns irrelevant for Q. In other cases, the Q may be affected by scattering losses, and ALD may participate in reducing these losses. Still, even in this case, the reduction of absorption is of comparable order of magnitude, and determines the change in thermo-optic shifts. Finally, in the last cases, ALD barely modifies scattering losses, while it strongly reduces absorption. In all cases, reduction of absorption by ALD plays a central role.

For ultrahigh-Q modes, like the ones reaching the high 10^5 and million range in this work, the situation is equivalent to the first cases. Prior to ALD these high-Q modes are not limited by scattering losses, but by surface absorption (see a complete study in [7]). Hence possible reduction of scattering losses by ALD only makes scattering loss have an even more negligible impact on Q, and it is the reduction of absorption that dominates the Q improvement.

Impact of the surface treatment on WGMs resonant wavelength. In order to understand the evolution of WGM resonant wavelengths, we numerically simulated the electromagnetic changes induced by the subsequent steps of the ALD surface treatment process. We used for the refractive index of alumina a commonly found value of n=1,7471. In [8], the refractive index of alumina deposited by ALD was measured for different deposition temperature, up to 180° C. Our growth temperature being of 300° C, these results extrapolate to a value of 1.7, consistent with the employed value. With this value in hands, axisymmetric FEM calculations allowed determining the WGMs wavelength shifts produced by ALD deposition. In order to compare these values to the experimentally measured shifts, one needs to evaluate the shifts produced by the surface preparation made prior to ALD itself. In our experiments, it consists (sometimes) in a dip in ammonia, followed (always) by a hydrogen plasma exposure. These steps not only remove the surface reconstruction layer (SRL), but also etch away some GaAs material, hence reducing the dimensions of the disks and shifting the optical resonances as well. Our past experience indicates that the removal of the mere surface reconstruction layer with a short dip in ammonia leads to reduce the dimensions of a GaAs disk by about 2 nm (radius and thickness) [7]. In the present work, the ammonia dips tend to be longer hence the amount of removed GaAs should be larger. Additionally the dips are performed manually, with variations in their duration and in the stirring conditions in the solution, such that a variation in the produced surface etching is also expected. The subsequent hydrogen plasma treatment, which is carried under more reproducible conditions, also contributes to the wavelength shift by etching away some GaAs, in a way that we are evaluating below.

On the disk of radius 4.5 µm employed in Fig. 3 (a) and (b), there is no ammonia treatment, but only a hydrogen plasma treatment followed by ALD. FEM simulations indicate that the ALD deposition of 30 nm of alumina experienced by this disk should red shift the TE WGMs resonance wavelengths by 19 (±1) nm. Of course, the exact amplitude of the shift depends on the radial and azimuthal number of each WGM (p=1 to 6 in the present case, corresponding to the variation of ±1 nm). Experimentally, this disk experiences a red shift of its WGM resonances by 9.5±2 nm (again for p=1 to 6). This means that the hydrogen-plasma treatment blue shifted the resonances by 9.5±3nm. FEM simulations indicate that such blue shift corresponds to the removal of a GaAs layer of thickness 2.3±0.7 nm all around the disk. Our hydrogen plasma process being reproducible; our understanding is that it always removes that same amount of GaAs on the surface. In Fig 2, the disk has a radius of 4.5 µm and it experiences first an ammonia pre-treatment. With the hydrogen plasma, our analysis from above shows that WGM resonances are blue shifted by 9.5±3nm. An ALD deposition of 30 nm red shifts the resonances by 19±1 nm. Experimentally, we measure a red shift of 2.4±1 nm, which means that our ammonia pre-treatment has induced a blue shift of 7.1±5 nm. According to our FEM simulations, this corresponds to the removal of a GaAs layer of thickness 1.7±1.2nm. This finding is consistent with our past experience on short dips of GaAs disks in ammonia [7]. On a disk of radius 3.4 µm, like the one employed in Fig. 3 (c) and (d), FEM calculations show that the hydrogen plasma produces a blue shift or resonances of 9.44±2.9 nm, and that an ALD of 20 nm of alumina produces a red shift of 14.3±1 nm. Because the measured shift for the disk employed in Fig. 3 (c) and (d) is a blue shift of 13.3±1.7 nm, we deduce that the long dip in ammonia experienced by this disk has generated a blue shift of 18.1±6.6 nm. According to our FEM calculations, this corresponds to the removal of a GaAs layer of thickness 4.4±1.6 nm. There again, this finding is consistent with our past experience on ammonia dips, even if this disk has visibly experienced a slightly more pronounced etching (longer dip duration, different stirring conditions).

Impact of the ALD thickness on the Q improvement. In Fig. 5 of the main text, data of Q improvement by ALD were reported without mentioning precisely the ALD thickness employed for each disk and for for each WGM. In Fig. S3, this thickness is reported, evolving between 5 and 30 nm. From the (limited) statistics gathered here, it seems that the beneficial features of the ALD appear already at the smallest thickness of 5 nm, and that a thicker amount of deposition is not required.

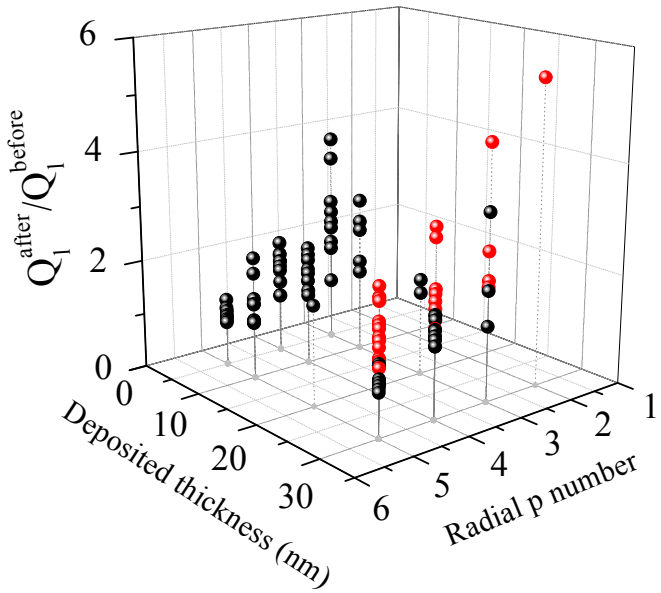

Fig. S3. Role of the alumina thickness in the Q improvement by ALD.

REFERENCES

1. V. L. Berkovits, V. P. Ulin, M. Losurdo, P. Capezzuto, G. Bruno, G. Perna, and V. Capozzi, Appl. Phys. Lett. 80, 3739 (2002).
2. V. L. Berkovits, V. P. Ulin, O. E. Tereshchenko, D. Paget, A.C.H. Rowe, P. Chiaradia, B.P. Doyle, and S. Nannarone, J. Electrochem. Soc. 158, D127 (2011).
3. V. L. Berkovits, L. Masson, I. V. Makarenko, V.P Ulin. Appl. Surf. Sci. 254, 8023 (2008).
4. P. A. Alekseev, M. S. Dunaevskiy, V. P. Ulin, T. V. Lvova, D. O. Filatov, A.V. Nezhdanov, A. I. Mashin, and V. L. Berkovits, Nano Lett. 15, 63 (2015).
5. A. Amo, M. D. Martín, L. Viña, A. I. Toropov, and K. S. Zhuravlev, Phys. Rev. B **73**, 035205 (2006).
6. A. Amo, "Carrier dynamics in semiconductors and semiconductor microcavities", PhD thesis, Universidad Autonoma de Madrid (2008).

7. D. Parrain, C. Baker, G. Wang, B. Guha, E. Gil-Santos, A. Lemaitre, P. Senellart, G. Leo, S. Ducci, and I. Favero, Opt. Exp. 23(15), 19656 (2015).
8. M. D. Groner, F. H. Fabreguette, J. W. Elam, and S. M. George, Chem. Mater. 16, 639-645 (2004).